Dendritic solidification microstructure affecting mechanical and corrosion properties of a Zn4Al alloy

WISLEI RIUPER OSÓRIO, CÉLIA MARINA A. FREIRE, AMAURI GARCIA*
Department of Materials Engineering,State University of Campinas, UNICAMP, P.O. Box 6122, 13083-970, Campinas, SP, Brazil
E-mail: amaurig@fem.unicamp.br

In the present article some important trends have been shown regarding the relationship between solidification variables, microstructure, mechanical and corrosion properties of Zn-4 wt%Al alloy castings. The aim of the present work is to investigate the influence of heat transfer solidification variables on the microstructure of Zn-4 wt%Al castings and to develop correlations with mechanical and corrosion properties. Experimental results include transient metal/mould heat transfer coefficient (h_i), secondary dendrite arm spacings (λ_2), corrosion potential (E_{Corr}), corrosion rate (i_{Corr}), ultimate tensile strength (σ_u) and yield strength (σ_y) as a function of solidification conditions imposed by the metal/mould system. It was found that a structural dendritic refinement provides both higher corrosion resistance and better mechanical properties for a hypoeutectic Zn4Al alloy.

1. Introduction

To address the increasing demand for high performance high quality die castings, a class of zinc based engineering cast alloys have been developed, in particular for applications in the automotive industry. Three members of this family of alloys are generally identified industry-wide as ZA-8, ZA-12 and ZA-27. The numerical components of the alloy designation indicate the approximate aluminum content. ZA-8 is the preferred choice for permanent mold castings and ZA-12/ZA-27 are usually cast in sand molds. Die casting is the process most often used for shaping zinc alloys [1]. The most commonly used zinc die casting alloys are those having 3.5–4.5 wt%Al, which will be referred as ZA-4 in the present study. The ZA alloys usually deliver high strength and superior hardness when compared to the most widely used non-ferrous alloys, combined with a good corrosion resistance.

Many analytical and numerical models were developed in the last 2 decades to treat heat transfer during solidification processes. The way the heat flows across the metal/mould system affects directly the evolution of solidification playing an important role in determining the freezing conditions inside the metal. As a direct consequence, solidification thermal parameters are strongly dependent on a wide range of operational conditions that may exist in foundry and casting processes. Control of solidification thermal parameters such as tip growth rate (V_L), thermal gradient (G_L), cooling rate (T), and local solidification time (t_{SL}) permits a range of microstructures to be obtained [2–4]. On the other hand, the morphological structure parameters such as grain size and interdendritic spacings also depend on heat transfer along the metal/mould system. As a consequence, there is a close correlation between thermal parameters and the solidification structure.

It is generally stated that as the grain size decreases, the metal strength increases. The Hall- Petch equation shows that the yield strength is proportional to the reciprocal of the square root of the grain diameter [5, 6]. For cast metals, however, it is not always true that the strength improves with decreasing grain size. Strength will increase with grain size reduction only if the production of small grains does not increase the amount of microporosity, the volume percent of second phase or the dendrite spacing [2, 9, 10].

Several experimental and analytical studies have reported the effects of dendrite arm spacings upon mechanical properties [2, 9–12]. Thus, the microstructural parameters, and particularly the dendrite arm spacings, can be even more important in prediction of mechanical properties than grain size. On the other hand, the structural morphologies also play an important role in corrosion behavior. A number of experimental studies described the effects of structure upon corrosion resistance in a number of processes such as conventional welding, and both hot dip and electrochemical coating methods [13,14], laser surface melting and alloying [15–18], PVD and CVD deposition techniques [19,20], i.e., any method in which the solidification process is

*Author to whom all correspondence should be addressed.
0022-2461
DOI: 10.1007/s10853-005-0852-z

relatively rapid to generate a finer solidification structure [21]. Therefore, it is clear that structural parameters including alloy content, porosity, grain size, dendrite spacing and both amount and homogeneity of distribution of second phases are important parameters that are also responsible for corrosion performance. Dendrite arrangement as a function of solidification parameters will be very important to evaluate both mechanical and corrosion resistance. The corrosion behavior will be defined by the morphological formation, interdendritic spacings, solute distribution, and anodic and cathodic characteristics.

1.1. Metal/mold heat transfer coefficient (h_i)

Heat flow across the metal casting/mold interface can be characterized by a macroscopic average metal/mold interfacial heat transfer coefficient (h_i), given by:

$$h_i = \frac{q}{A\,(T_{\mathrm{IC}} - T_{\mathrm{IM}})} \tag{1}$$

where q [W] is the average heat flux, A [m^2] is area and T_{IC} and T_{IM} are metal and mold surface temperatures [K] at the interface. It is well known, that during the solidification process, the mold gradually expands due to heat absorption, and the metal casting is subjected to shrinkage. As a result, a gap develops due to insufficient contact between metal and mold, and as a direct consequence, h_i decreases rapidly. In a previous article the transient interfacial heat transfer coefficient has been successfully characterized by using an approach based on measured temperatures in casting and numerical simulation provided by a heat transfer model [22]. This coefficient has been expressed as a power function of time, given by:

$$h_i = C_i\,(t)^{-n} \tag{2}$$

where h_i [W/m^{2}K], t is the time [s] and C_i and n are constants which depend on alloy composition, chill material and superheat. Santos *et al.* [22] have reported the effects of alloy composition, chill material, chill thickness and melt superheat upon the metal/mold heat transfer coefficient (h_i).

1.2. Thermal solidification variables and dendrite arm spacing

An analytical heat transfer model describing temperature distribution and the displacement of solidus and liquidus isotherms during the unidirectional solidification of binary alloys, can be used for determining expressions for thermal variables, such as tip growth rate (V_L), temperature gradient (G_L), tip cooling rate (T_L) and local solidification time (t_{SL}) as a function of the metal/mold system and consequently, as a function of metal/mold heat transfer coefficient [2, 4, 23, 24]. Particularly, the tip growth rate is given by:

$$V_L = \frac{2\alpha_{\mathrm{SL}}\phi_2^2}{\left[\frac{2k_S\phi_2(T_{\mathrm{Sol}}-T_0)}{n\sqrt{\pi}(T_{\mathrm{Liq}}-T_0)\exp(\phi_1^2)[M+\mathrm{erf}(\phi_1)]h_i}\right] + S_L} \tag{3}$$

where α_{SL} is the thermal diffusivity of mushy zone, ϕ_1 and ϕ_2 are solidification constants [2, 4] associated to the displacement of solidus and liquidus isotherms, respectively, k_S is the solid thermal conductivity, T_{Sol} is the non-equilibrium solidus temperature, T_0 is the environment temperature, T_{Liq} is the liquidus temperature, M is the ratio of heat diffusivities of solid and mold material, $(k_S c_S \rho_S / k_M c_M \rho_M)^{1/2}$, n is the square root of the ratio of thermal diffusivities of solid metal and mushy zone, $(\alpha_S/\alpha_{\mathrm{SL}})^{1/2}$, S_L is the position of liquidus isotherm from metal/mold interface and h_i is the metal/mold heat transfer coefficient Equation 3 has been validated against experimental data describing the unidirectional solidification of Al-Cu; Sn-Pb [2–4 , 25] and Zn-Al [9] alloys.

A number of solidification studies have been developed with a view to characterizing dendrite spacing under experimental circumstances involving solidification in steady-state heat flow and those in the unsteady-state regime [2–4, 25–32]. The latter case is of prime importance, since this class of heat flow regime encompasses the majority of industrial solidification processes. In the unsteady-state case, dendrite spacings λ_1 and λ_2, are usually expressed as a function either of cooling rate, $\dot{\mathrm{T}}_L$, or local solidification time, t_{SL}, according to:

$$\lambda_{1,2} = C_{\mathrm{i}}(GV)^{-a} \tag{4}$$

or

$$\lambda_2 = K\,(t_{\mathrm{SL}})^{\mathrm{a}} \tag{5}$$

where C_i are constants, and the exponent a has been recently summarized in the literature for a number of alloys [26]. Recently, experimental and theoretical studies [2, 4, 9, 10] have also been reported where primary and secondary dendrite spacings, λ_1 and λ_2 respectively, are expressed as a function of V_L or $\dot{\mathrm{T}}_L$ for unsteady-state solidification conditions.

The correlation of mechanical and corrosion behavior with microstructure parameters can be very useful for planning solidification conditions in terms of a determined level of mechanical and corrosion properties which are desired.

The present work focuses on the influence of heat transfer on solidification microstructure of Zn-4 wt%Al castings and the correlation with mechanical and corrosion resistance. Experimental results include transient metal/mould heat transfer coefficient (h_i), secondary dendrite arm spacings (λ_2), corrosion potential (E_{Corr}) and rate (i_{Corr}), ultimate tensile strength (σ_u) and yield strength (σ_y) as a function of solidification conditions imposed by the metal/mould system.

TABLE I Mean chemical composition of Zn and Al

Zinc (Mean chemical composition)					
Element	Zn	Fe	Pb	Si	Other
(wt%)	99.97	0.015	0.012	0.003	–
Aluminum (Mean chemical composition)					
Element	Al	Fe	Pb	Si	Other
(wt%)	99.93	0.038	<0.001	0.033	–

2. Experimental procedure

Fig. 1a shows the casting assembly used in solidification experiments [2, 9]. The main design criterion was to ensure a dominant unidirectional heat flow during solidification. This objective was achieved by adequate insulation of the chill casting chamber. A low carbon steel chill was used at a normal environment temperature of about 25 °C (initial mold temperature), with the heat-extracting surface being polished. The ZA4 alloy (in this study ZA4 refers to the Zn-4 wt%Al alloy) was melted in an electric resistance-type furnace, degassed and then poured into the casting chamber with a melt pouring temperature of about 10 pct above the liquidus temperature (430 °C). This alloy was prepared by using commercially pure Zn and Al ingots. Table I shows the chemical composition of Zn and Al.

Temperatures in both metal and mold were monitored during solidification using a bank of type *J* and *K* thermocouples accurately located with respect to the metal/mold interface. All the thermocouples were connected by coaxial cables to a data logger interfaced with a computer, and the temperature data were acquired automatically. Fig. 1b exhibits both the longitudinal and the transversal specimens that were taken for optical metallographic examination and tensile testing, respectively, according to specifications of ASTM Standard E 8M. Longitudinal specimens were obtained from the solidified casting with the selected section being polished and etched to reveal the microstructure. The etchant used was a solution containing 5 g CrO_3, 0.5 g Na_2SO_4 and 100 ml H_2O and rinsed in a solution of 20 g CrO_3 and 100 ml H_2O before optical microscopy examination [31]. An image processing system, was then used to measure the average secondary dendrite arm spacings for each selected position. To ensure reproducibility of results, four specimens were tested for each selected position, and mean values of yield and ultimate tensile strengths were determined at different positions with respect to the metal/chill interface.

Although accelerated corrosion testing is widely used since the early 1900s [33], for some particular situations, the excessive aggressiveness of such a test could mask the real material performance at the initial stage of corrosion [34]. In the present experimental investigation the electrochemical technique and the polarization method were chosen to investigate the material corrosion performance. Electrochemical impedance spectroscopy (EIS) tests were conducted in a 3% NaCl solution at room temperature by using a, potentiostat coupled to a frequency analyzer system, a glass corrosion cell kit with a platinum counter electrode and a saturated calomel reference electrode (SCE), as prescribed by the ASTM standard G3 [35]. The working electrodes consisted of cast ZA4 samples. Polarization tests were also conducted in a 3% NaCl solution at room temperature using the above-mentioned potentiostat, by stepping the potential using a scanning rate of 0.2 mV/sec from –250 mV (SCE) to +250 mV(SCE) related to open-circuit potential. The polarization curves were plotted and both current density and corrosion potential were calculated by Tafel extrapolation method [36–39]. The EIS tests were performed in a frequency range between 100 mHz and 100 kHz. Before each corrosion test, the samples were ground up to a 600 SiC grit paper, cleaned by distilled water and dried by airflow.

3. Results and discussion

The experimentally monitored temperatures were compared with theoretical predictions of a finite difference

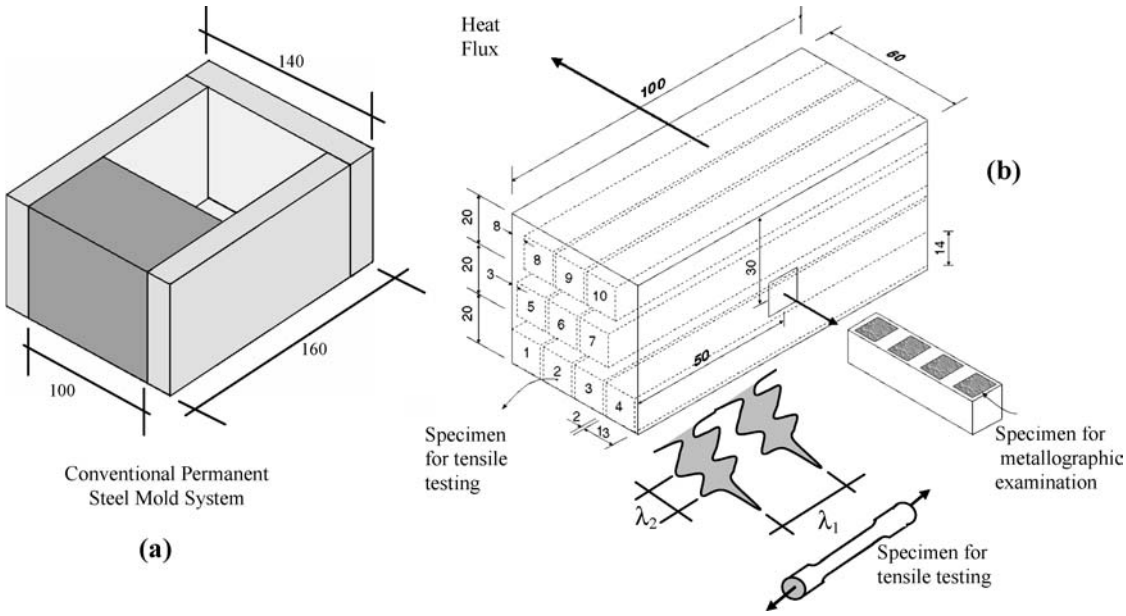

Figure 1 Casting assembly (a) and location of specimens for metallographic examination and tensile testing (b).

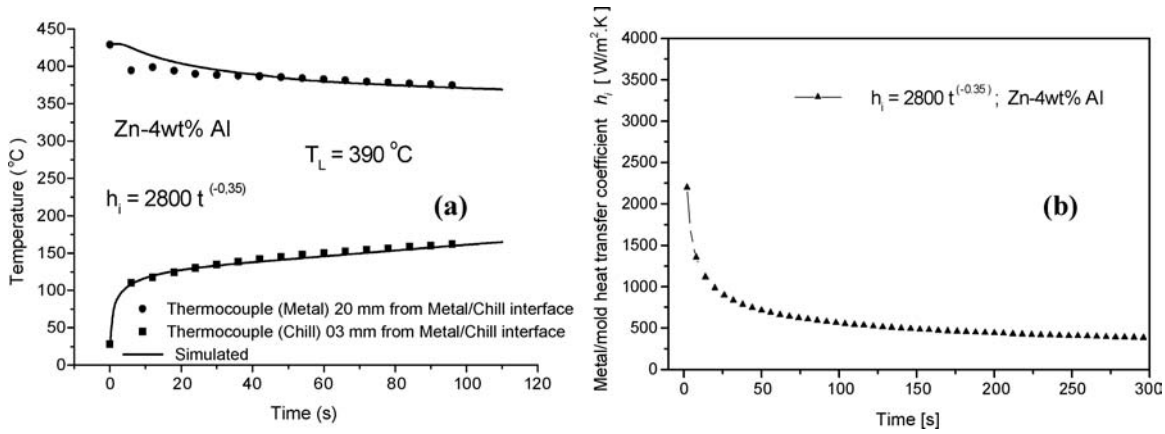

Figure 2 Typical experimental thermal responses compared to numerical simulations (a) and transient metal/mold heat transfer coefficients, h_i [W/m^2 K] (b) as a function of time.

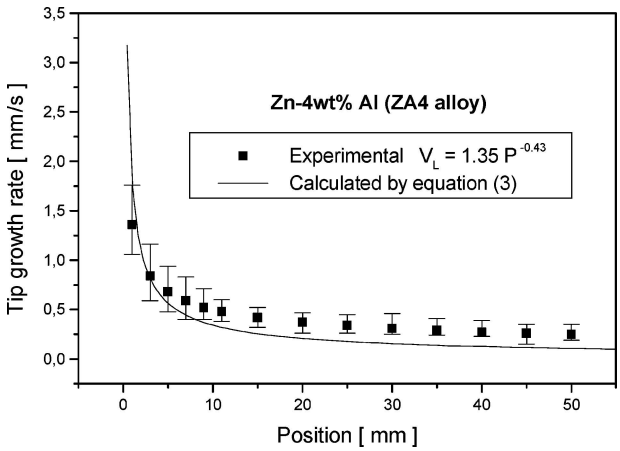

Figure 3 Comparison between experimental and calculated tip growth rate (V_L) as a function of position from the metal/mold interface.

heat flow model to determine the transient metal/mold heat transfer coefficient (h_i) [3, 4, 9, 22]. Fig. 2 shows the typical experimental results of thermal responses compared with those numerically simulated and the resulting h_i coefficient profiles as a function of time. It is known that the chemical composition and superheat affects h_i profiles [4, 22]. For the present experiment the adopted melt superheat was about 10% of the liquidus temperature.

The results of experimental thermal analysis inside the casting have also been used to determine the tip growth rate (V_L), as a function of time and/or position. The thermocouples readings have been used to generate a plot of position from the metal/mold interface as a function of time corresponding to the liquidus front passing by each thermocouple. A curve fitting technique on these experimental points has generated a power function of position as a function of time. The derivative of this function with respect to time has yielded values for tip growth rate. Fig. 3 shows a comparison between the experimental and calculated tip growth rate as a function of position from the metal/mold interface. The calculated tip growth rate was obtained by using the analytical expression given by Equation 3. In this equation, the appropriate experimental values of h_i coefficient, given in Fig. 2, and the thermophysical properties reported in a previous article [9] were used. Good agreement can be observed between theoretical and experimental results. The verified deviations are mainly caused by: (i) uncertainties

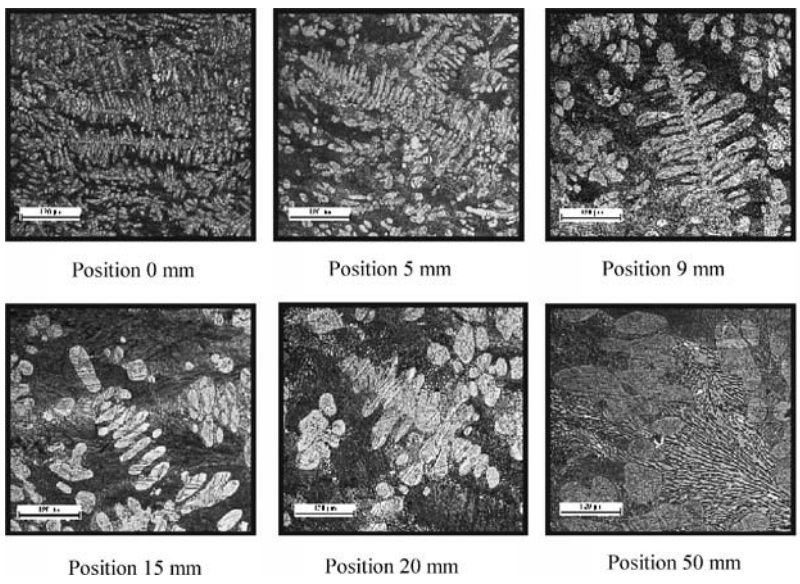

Figure 4 Typical microstructures for a ZA4 alloy at different positions from the metal/mold interface.

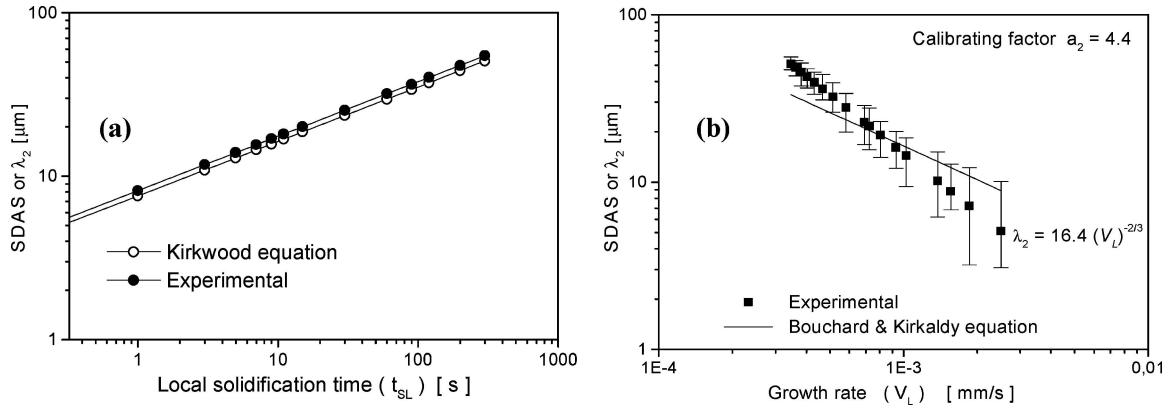

Figure 5 Comparison between experimental and theoretical λ_2 (Kirkwood and Bouchard/Kirkaldy equations) versus local solidification time (a) and tip growth rate (b) for a ZA4 alloy.

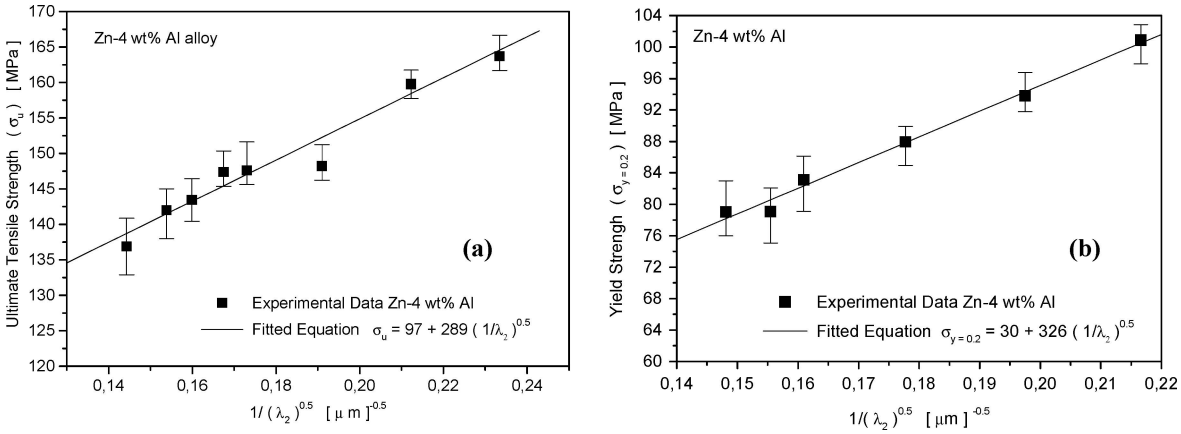

Figure 6 Ultimate tensile strength (UTS) (a) and Yield Strength (YS) (b) as a function of secondary dendritic arm spacings (λ_2 or SDAS) for a ZA4 alloy.

in the thermophysical properties, which were adopted as proportional values calculated from the properties exhibited by each metal, and (ii) the presence of convection currents in the liquid metal induced by fluid motion during pouring which were not considered by the analytical model.

Fig. 4 exhibits typical ZA4 microstructures at different locations from the metal/mold interface. As expected, with increased distance from the casting surface, the secondary dendrite arm spacings (λ_2) increase due to the decrease in cooling rate.

Fig. 5a presents a comparision between experimental and calculated values of λ_2 as a function of local solidification time by using the model proposed by Kirkwood [28]. An excellent agreement can be observed. Fig. 5b illustrates a comparison between experimental and calculated λ_2 parameter versus tip growth rate. The theoretical approach was that due to Bouchard and Kirkaldy [26]. A reasonable to good agreement can be observed. The analytical expression for the tip growth rate, given by Equation 3 can be incorporated into the Bouchard and Kirkaldy equation such that λ_2 can be expressed as a function of metal/mold heat transfer coefficient and other solidification operational parameters [9, 10].

Fig. 6 shows the experimental results of UTS and Yield Strength (0.2% proof stress) as a function of secondary dendrite arm spacing. The results are consistent

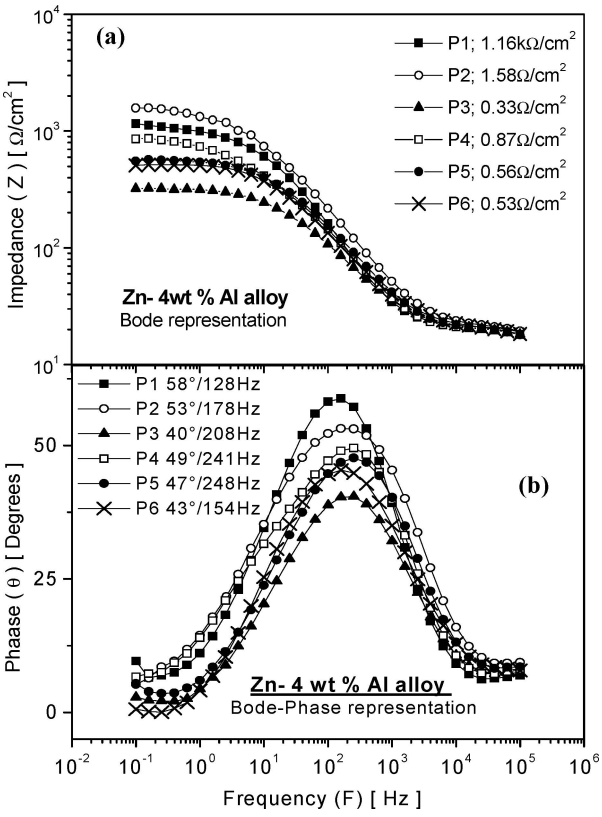

Figure 7 Results of EIS tests in: Bode (a), Bode-Phase (b) representation for Zn-4 wt% Al.

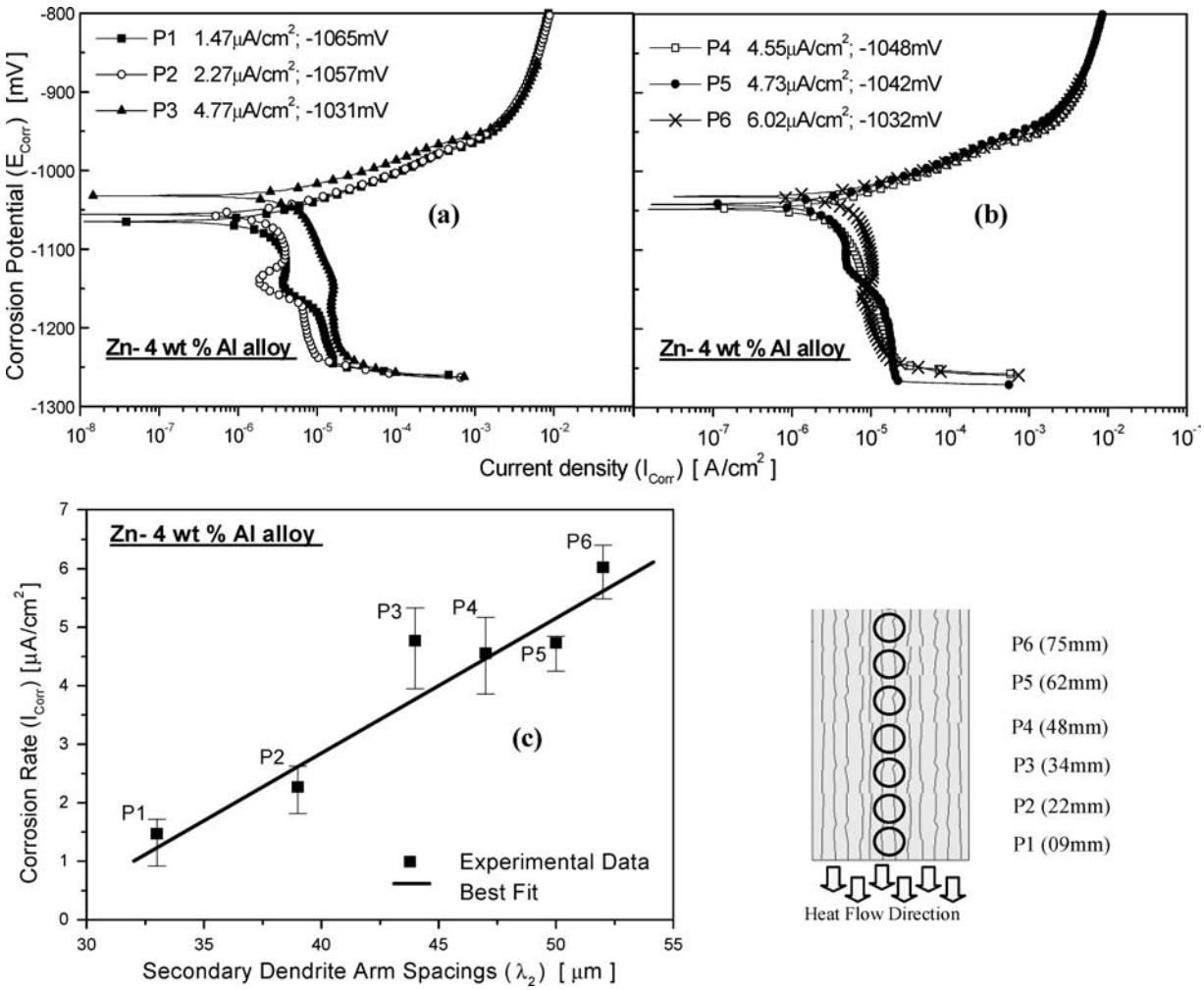

Figure 8 Experimental results of potentiodynamic polarization curves (a and b) and Zn-4 wt% Al corrosion resistance tendency as a function of position from the metal/mold interface (c).

with those found in the literature concerning Zn-Al commercial alloys [11].

Analysis of the above experimental results has yielded equations, as indicated in Fig. 6, relating the dependence of *UTS* and YS on secondary dendrite arm spacings. It can be seen that a finer structural morphology provides better mechanical properties than a coarser morphology. These equations can incorporate models expressing λ_2 as a function of thermal solidification variables and metal/mold heat transfer coefficient permitting expressions correlating mechanical properties with solidification conditions to be established [9].

Fig. 7 shows experimental corrosion results for the ZA4 alloy. Fig. 7a and b show the *Bode* and *Bode-Phase* representation respectively, for different positions from the metal/mold interface.

Fig. 8a–c show, respectively, the experimental polarization curves and tendency of the corrosion rate as a function of secondary dendrite arm spacings. The final structure of hypoeutectic Zn-Al alloys, immediately after solidification will be formed by a phase α, which is the dendritic matrix (solid solution of Al in Zn) involved by an interdendritic eutectic lamellar mixture consisting of the phases α and β (solid solution of Zn in Al). During subsequent cooling a eutectoid decomposition will take place, and at temperatures below the eutectoid the phase β transforms to a eutectoid mixture of $(\alpha + \beta)$. This will affect only the composition of the phase β inside the lamellar structure, but the dendritic matrix will not affected since the phase α will not be subjected to any solid-state transformation. Fig. 9 shows the observed lamellar eutectic structure.

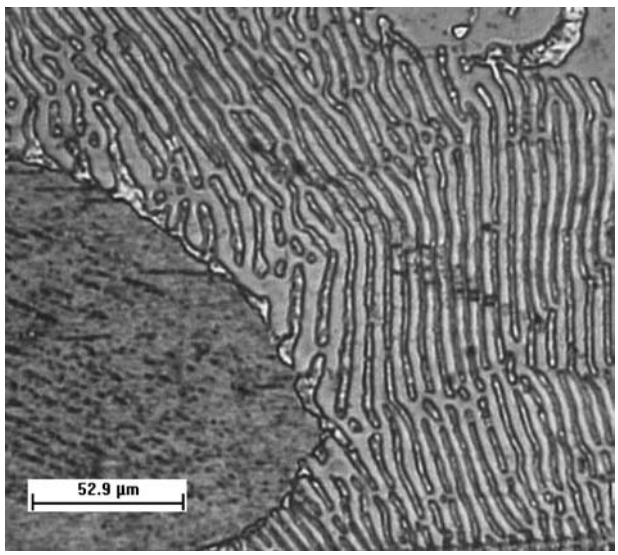

Figure 9 Typical eutectic lamellar morphology observed at the interdendritic regions of Zn-Al alloys.

The beneficial effect of aluminum for corrosion resistance of Al-rich phase of cast alloys has been reported in a recent study [40]. In the lamellar eutectic morphology, the phase β (Al-rich) is so close to the phase α that it acts as a barrier to corrosion. So, if we provide a eutectic layer to protect the dendritic matrix (Zn-rich), this can help corrosion resistance. This will be more effective for smaller dendritic arm spacings, i.e., a more extensive distribution of the "protective" barrier will be provided. It is important to remark that the amount of eutectic in commercial Zn-Al hypoeutectic alloys is high, e.g., for a Zn 4 wt%Al alloy, using Scheil's equation: 76% eutectic and 24% α.

4. Conclusions

In this study, the role of heat transfer on solidification microstructure of a Zn-4Al alloy and the correlation with mechanical and corrosion properties has been analyzed. The following conclusions can be drawn.

(1) The comparison between experimental and calculated λ_2 as a function of the thermal solidification variables, such as, the local solidification time and tip growth rate has shown that the experiments are in good agreement with both Kirkwood and Bouchard/Kirkaldy theoretical models.

(2) The experimental expressions correlating the *UTS* and YS with λ_2 for a ZA4 alloy have shown that a finer structural dendritic morphology provides better mechanical properties than a coarser morphology.

(3) The experimental corrosion tests results have shown that for a hypoeutectic Zn4Al alloy, in which interdendritic regions contain Aluminium-rich solution as one of the phases of a lamellar eutectic mixture, finer dendritic structures tend to yield higher corrosion resistance than coarser dendritic structures.

(4) The control of dendritic as-cast microstructures, by manipulating solidification processing variables, can be used as an alternative way to produce components with higher corrosion resistance and better mechanical properties.

Acknowledgements

The authors acknowledge financial support provided by FAEP-UNICAMP, FAPESP (The Scientific Research Foundation of the State of São Paulo, Brazil) and CNPq (The Brazilian Research Council).

References

1. C. H. DALE, in *Metals Handbook*, Vol. 15 *Casting* (edited by ASM International, Metals Park, OH, USA, 1988) p. 786.
2. J. M. V. QUARESMA, C. A. SANTOS and A. GARCIA, *Metall. Mat. Trans. A* **31** (2000) 3167.
3. C. A. SIQUEIRA, N. CHEUNG and A. GARCIA, *ibid.* **33** (2002) 2107.
4. O. L. ROCHA, C. A. SIQUEIRA and A. GARCIA, *ibid.* **34** (2003) 995.
5. E. O. HALL, *Proc. Phys. Soc.*, **71B** (1951) 747.
6. N. J. PETCH, *J. Iron* and *Steel Institute* **174** (1953) 25.
7. J. T. BERRY, *AFS Transactions* **78** (1970). 421.
8. P. DONELAN, *Mat. Sci. Tech.* **16** (2000) 261.
9. W. R. OSÓRIO and A. GARCIA, *Mater. Sci. Eng. A* **325** (2002) 103.
10. W. R. OSÓRIO, C. A. SANTOS, J. M. V. QUARESMA and A. GARCIA, *J. Mat. Proc. Tech.* **143** (2003) 703.
11. M. DURMAN, *Z. Metalkd.* **89** (1998) 417.
12. M. A. SAVAS and S. ALTINTAS, *J. Mater. Sci.* **28** (1993) 1775.
13. H. PARK and J. A. SZPUNAR, *Corr. Sci.* **40** (1998) 525.
14. P. R. SERÉ, J. D. CULCASI, C. I. ELSNER and A. R. DI SARLI, *Surf. Coat. Technol.* **122** (1999) 143.
15. K. G. WATKINS, M. A. MCMAHON and W. M. STEEN, *Mater. Sci. Eng.* A **231** (1997) 55.
16. T. T. WONG and G. Y. LIANG, *J. Mat. Proc. Tech.* **63** (1997) 930.
17. J. K. SHIN, J. H. SUH, J. S. KIM and S. J. L. KANG, *Surf. Coat. Technol.* **107** (1998) 94.
18. A. CONDE, R. COLAÇO, R. VILAR and J. DE DAMBORENEA, *Mat. Design* **21** (2000) 441.
19. I. GARCIA and J. J. DE DAMBORENEA, *Corr. Sci.* **40** (1998) 1411.
20. M. A. BAKER, W. GISSLER, S. KLOSE, M. TRAMPENT and F. WEBER, *Surf. Coat. Technol.* **125** (2000) 207.
21. G. SONG, A. ATRENS and M. DAREUSCH, *Corr. Sci.* **41** (1999) 249.
22. C. A. SANTOS, J. M. V. QUARESMA and A. GARCIA, *J. Alloys Compd.* **319** (2001) 174.
23. A. GARCIA, T. W. CLYNE and M. PRATES, *Metall. Trans.* **10B** (1979) 773.
24. A. GARCIA and T. W. CLYNE, in Proceeding of International Conference on Solidification Technology in the Foundry and Casthouse, London, september (edited by The Metals Society, 1980) p. 33.
25. F. SÁ, O. L. ROCHA, C. A. SIQUEIRA and A. GARCIA, *Mater. Sci. Eng.* A **373** (2004) 131.
26. D. BOUCHARD and J. S. KIRKALDY, *Metall. Mat. Trans.* **28B** (1997) 651.
27. J. S. KIRKALDY and D. VENUGOPALAN, *Scrip. Met.* **23** (1989) 1603.
28. D. H. KIRKWOOD, *Mat. Sci. Eng* **73** (1985). L1.
29. J. D. HUNT and S. Z. LU, *Metall. Mat. Trans.* **27A** (1996) 611.
30. V. LAXMANAN, *Scri. Mat.* **38** (1998) 1289.
31. N. TUNCA and R. W. SMITH, *J. Mat. Sci.* **23** (1988) 111.
32. W. KURZ and J. D. FISHER, *Act. Met.* **29** (1981) 11.
33. C. L. MEADE, *Met. Finish.* **98** (2000) 540.
34. A. CONDE and J. DE DAMBORENEA, *Corr. Sci.* **39** (1997) 295.
35. ASTM G3—*Standard Recommended Practice for Conventions Applicable to Electrochemical Measurements in Corrosion Tests* (1988).
36. M. STERN and A. L. GEARY, *J. Electroch. Soc.* **4** (1957) 56.
37. W. R. OSÓRIO, C. M. A. FREIRE and A. GARCIA, in Proceeding of 18th SMT/International Conference on Surface Modification Technology, Dijón, France, Nov. 2004, edited by T. S. Sudarshan.
38. W. R. OSÓRIO, C. M. A. FREIRE and A. GARCIA, in Proceeding of 15th ICC/International Corrosion Congress, Granada, Spain, Sept. 2002.
39. Idem., in Proceeding of IX International Conference on Metallurgical Science and Technology, Madrid, Spain, Oct. 2003, edited by CENIN, pp. 32 and 50.
40. G. SONG, A. L. BOWLES and D. H. ST. JOHN, *Mater. Sci. Eng.* A **366** (2004) 74.

Received 9 December 2004
and accepted 7 March 2005